A MULTI-FLUID MODEL OF TURBULENCE FOR L_i-SF_6 SUBMERGED COMBUSTION

S. H. Chan and M. M. M. Abou-Ellail
Department of Mechanical Engineering
University of Wisconsin--Milwaukee
P.O. Box 784
Milwaukee, Wisconsin 53201

TECHNICAL REPORT

Prepared for the Department of the Navy
Office of Naval Research
Arlington, VA 22217

Under Contract No.: N00014-89-J-1267 (Oct. 1988 - Feb. 28, 1993)
For the period: July 15, 1991 - August 1, 1991

August 1, 1992

C2:multi-fl

TABLE OF CONTENTS

ABSTRACT

Liquid metal combustion has been used as the primary energy source for underwater vehicle propulsion because of its energetic and closed-cycle characteristics. This can be achieved by injecting gaseous oxidizer (SF_6) in a molten metal (Li) bath. The present paper describes a new multi-fluid (MF) combustion model for multiphase submerged diffusion flames. Each fluid has separate transport equations which are linked to other fluids' transport equations by additional source terms. The present MF model results for a submerged $Li(\ell)$-$SF_6(g)$ flame gave a much longer plume length compared to the corresponding locally-homogeneous flow (LHF) model results and is in good agreement with the experimentally measured plume length.

ACKNOWLEDGEMENT

This research was sponsored by the U.S. Office of Naval Research, Grant No. N00014-89-J-1267, under the technical management of Dr. G. Roy.

LIST OF FIGURES

1. INTRODUCTION

Stored chemical energy propulsion systems (SCEPS) using Li/SF_6 reactants have recently received a great deal of attention as a means of producing high energy per unit mass of reactant [1-9]. The "SCEPS" system utilizes a liquid-metal fuel combustor as part of a closed steam-power cycle. The combustor uses a liquid metal bath (fuel) through which a high-momentum gas jet (oxidizer) is injected forming a reacting multiphase submerged jet. Lithium (Li) has been used as the liquid metal while sulfur hexafluoride (SF_6) gas or other halogen gas is used as the oxidant. In this case, flame temperatures as high as 4000 K may be encountered making detailed flame structure measurements currently very difficult, if not practically impossible.

Computer simulation of liquid metal fuel combustors has recently been adopted as the next possible technique for obtaining detailed information regarding the multiphase submerged flame structure [1-11]. All the current computational models use the LHF model as a basis for predicting the submerged diffusion flame with the obvious assumption of infinitely fast transport mechanisms [phase equilibrium and same velocity and temperature of all phases, etc.] between the reacting phases. This very assumption leads to a substantially underpredicted plume length for the Li-SF_6 submerged flame [9].

Presently, other than the LHF model, very few combustion models can be used to predict the turbulence structure of multiphase submerged reacting plumes. Practically all the contemporary non-submerged models (stochastic separated-flow model, etc.) developed for liquid-fuel spray flames are unfortunately inapplicable to the submerged reacting plumes because of the flow regime change and condensation of products and excess evaporated fuel. When a gaseous oxidant is injected into a liquid fuel, the flow regime begins with a single-phase, gaseous flow pattern at the nozzle exit. As the liquid fuel is entrained to

react with the oxidant, a liquid droplet flow pattern may evolve first. However, the mixture temperature is still low enough that the product may appear in a solid phase [9] such that the droplet flow regime may be composed of gas, liquid and solid phases. Further downstream, with sufficient entrainment and reaction, a gaseous flow pattern may reappear, which may be followed by another droplet flow and then a bubbly flow pattern due to condensation of vapor products and excessively evaporated fuel vapor. Eventually it should turn into condensed phases at the tip of the plume. Though the above description of flow patterns may be rather speculative, the submerged reacting jets are therefore distinctly different from the better known two-phase spray jets, in which droplets from the spray nozzle simply evaporate and react to form non-condensable gaseous products with no subsequent condensation. It is somewhat similar to the conventional two-phase flow, see for example Ishii [12], in which the void fraction can range between zero and one, flow regimes can change and the interaction between two phases is strong. Consequently, the continuum concept of the two-fluid model in the field of two-phase flow is adopted. However, it is necessarily extended to reacting multiphase flow to account for not only velocity slip between phases but also phase nonequilibrium between phases and turbulence-reaction interaction through a PDF (probability density function) approach. The results are compared with that of the prevailing LHF model and available experimental data to validate the proposed model for multiphase submerged combustion.

2. THE PHYSICAL MODEL

The proposed physical model treats the multiphase submerged flame as a number of "fluids" or phases (i.e., fluid 1, fluid 2, ..., fluid k, ..., fluid n). The total number of fluids is n; any flow or thermochemical property (ϕ) pertaining to fluid k ($1 \leq k \leq n$) is designated by a "k" superscript, e.g., ϕ^k). The last two fluids (fluid (n-1) and fluid n) are respectively dispersed

condensed combustion products (such as LiF(ℓ), $Li_2S(\ell)$ and LiF(s)) and a continuous gas phase (such as $SF_6(g)$, Li(g), $Li_2F_2(g)$, $Li_3F_3(g)$ and $Li_2S(g)$, etc.). The remaining fluids ($1 \leq k < (n-2)$) are dispersed Li droplet phases; each fluid is characterized by a mean droplet diameter D^k, with the smallest diameter at $k = 1$. For compactness, all the modeled time-averaged, steady-state, conservation equations given below are expressed in compact tensor notation although they are actually solved in their cylindrical polar form. In the governing equations, terms involving ρ' were ignored. In the limit of phase equilibrium and non-slip between phases, the equations reduce to the Favre-averaged form of the LHF approximation [8].

a) **The mass conservation equation for fluid k:**

$$(\bar{\rho}^k \bar{\alpha}^k \bar{u}_i^k - (\mu_t^k/\sigma_\alpha^k)\, \bar{\alpha}^k_{,i})_{,i} = \dot{S}_m^{'''k} \tag{1}$$

where the comma suffix denotes differentiation with respect to the spatial coordinates, μ^k_t is the turbulent viscosity of fluid k; σ^k_α is a turbulent Schmidt number; $\bar{\alpha}^k$ is the mean volume fraction of fluid k; $\bar{u}^k_i$ is the mean velocity in the i-direction; $\bar{\rho}^k$ is the density; $\dot{S}_m^{'''k}$ is a volumetric mass source term because of mass transfer between the fluids due to evaporation, condensation and droplet inter-fluid transfer as droplets decrease in size. $\dot{S}_m^{'''k}$ is given as,

$$\dot{S}_m^{'''k} = \dot{m}^{'''k+1} \bar{\alpha}^{k+1} - (\dot{m}^{'''k} + \dot{m}_v^{'''k})\, \bar{\alpha}^k \qquad (1 \leq k \leq (n-2)) \tag{2}$$

and for $k = n$ (carrier fluid)

$$\dot{S}_m^{'''k} = \sum_{\ell=1}^{n-1} \dot{m}_v^{'''\ell} \bar{\alpha}^\ell - \dot{m}^{'''k} \bar{\alpha}^k \qquad (k = n) \tag{3}$$

In the above $\dot{m}'''^{k+1}$ is the volumetric liquid phase mass transfer from fluid (k+1) to fluid k. It can represent, for example, the rate of mass of droplets in size (k+1) group that is shifted to size (k) group due to evaporation. Similarly, $\dot{m}'''^{k}$ is the mass flowing out (as liquid phase) from fluid k and $\dot{m}_v'''^{k}$ is the evaporation rate. For the condensing combustion products (k=n-1) Equation (1) is actually used to compute the condensation rate source term $\dot{S}_m'''^{(n-1)}$ as will be explained later in Section 2.5. The last term in Equation (3) represents the condensation rate which is a loss of mass from the carrier phase to the (n-1) phase, assuming that the reaction has taken place in the gas phase only.

b) **Modeled momentum equation:**

$$[\bar{\rho}^k\bar{\alpha}^k\bar{u}_i^k\bar{u}_j^k - \bar{\alpha}^k(\mu_\ell^k + \bar{\rho}^k\nu_t/\sigma^k)(\bar{u}_{i,j}^k + \bar{u}_{j,i}^k - \tfrac{2}{3}\bar{u}_{m,m}^k\delta_{ij}) - \tfrac{2}{3}\bar{\rho}^k k^k\delta_{ij} - \bar{\rho}^k\nu_t^k(\bar{u}_i^k\bar{\alpha}_{,j}^k + \bar{u}_j^k\bar{\alpha}_{,i}^k)/\sigma_\alpha^k]_{,i} = -\bar{\alpha}^k\bar{p}_{,j} + \bar{F}_{Dj}^k + \bar{F}_{mj}^k + \bar{\alpha}^k(\bar{\rho}^k - \rho_o)\, g_j \qquad (4)$$

where, k^k is the turbulence kinetic energy; $\sigma^k = \nu_t/\nu_t^k$; ν_t and $\nu^k{}_t$ are the kinematic turbulent viscosities of the carrier phase (k=n) and fluid k; the mean drag and mass transfer forces $\bar{F}^k{}_{Dj}$ and $\bar{F}^k{}_{mj}$ may be given as follows for $1 \le k \le n - 1$ (dispersed fluids)

$$\bar{F}_{Dj}^k = f_D^k[\bar{\alpha}^k(\bar{u}_j^n - \bar{u}_j^k) + (1 - \sigma^k\sigma_\alpha^k/\sigma_\alpha^n)\,\nu_t^k\bar{\alpha}_{,j}^k/\sigma_\alpha^k] \qquad (5)$$

$$\bar{F}_{mj}^k = \dot{m}'''^{k+1}(\bar{\alpha}^{k+1}\bar{u}_j^{k+1} - \nu_t^{k+1}\bar{\alpha}_{,j}^{k+1}/\sigma_\alpha^{k+1}) - (\dot{m}'''^{k} + \dot{m}_v'''^{k}) \bullet (\bar{\alpha}^k\bar{u}_j^k - \nu_t^k\bar{\alpha}_{,j}^k/\sigma_\alpha^k) \qquad (6)$$

and for k = n (carrier fluid)

$$\bar{F}_{Dj}^k = -\sum_{\ell=1}^{n-1}\bar{F}_{Dj}^\ell \qquad (7)$$

$$\bar{F}^k_{mj} = \sum_{\ell=1}^{n-1} \dot{m}^{\ell}_{v} \left(\bar{\alpha}^{\ell}\bar{u}^{\ell}_{j} - \nu^{\ell}_{t}\bar{\alpha}^{\ell}_{,j}/\sigma^{\ell}_{\alpha}\right) \tag{8}$$

Finally, the global continuity must be included

$$\sum_{k} \bar{\alpha}^k = 1 \tag{9}$$

In the above equations, σ^k ($\equiv \nu_t/\nu^k{}_t$) is a turbulent Schmidt number; $\mu^k{}_\ell$ is the molecular viscosity; g_j is the gravitational acceleration in the j-direction; ρ_o is a reference density; p is the pressure; $f^k{}_D$ is a drag function which may be written as [13]

$$f^k_D = 18\ Z\ \mu^n_\ell/(D^k)^2 \qquad (1 \le k < n) \tag{10}$$

where D^k is a mean droplet size of "fluid k"; $\mu_\ell{}^n$ is the carrier phase molecular viscosity (i.e., for k = n); Z is a function of the droplet Reynolds number Re^k [13] and the droplet transfer number B [14]

$$Z = [1 + 0.15\ (Re^k)^{0.687} + 0.02\ Re^k/(1 + 42500/(Re^k)^{1.16}]/$$
$$(1 + B)^{0.25} \tag{11}$$

where, $Re^k \equiv \bar{\rho}^n D^k |\bar{u}^n_j - \bar{u}^k_j|/\mu_\ell$; $\bar{\rho}^n$ is the carrier phase density.

The turbulent Schmidt number, σ^k, reflects the coupling effect between the gas and liquid momentum fields. It can be calculated as [15]

$$\sigma^k = 1 + \frac{2}{3}\bar{\rho}^k\epsilon/[c_\mu k f^k_D(1+\bar{\alpha}^k\rho^k/\bar{\rho}^n\bar{\alpha}^n)] \quad (k\neq n) \tag{12}$$

and for k = n, σ^k = 1 by definition.

In the transport equations, only second order correlation terms (e.g., $\overline{u_i'^k u_j'^k}$, $\overline{\alpha'^k u_i'^k}$, $\overline{\alpha'^k u_i'^n}$) were retained [16].

2.1 The Turbulence Model

A multi-fluid k-ϵ model is adopted where transport equations for the kinetic energy of turbulence k and its dissipation rate ϵ, of the carrier fluid, are solved [17], namely

$$\bar{\rho}^n\bar{\alpha}^n\bar{u}_i^n k_{,i} - [(\mu_t\bar{\alpha}^n/\sigma_k) k_{,i}]_{,i} = \bar{\alpha}^n (G + \Delta G) - \bar{\rho}^n\bar{\alpha}^n (\epsilon + \Delta\epsilon) \quad (13)$$

$$\bar{\rho}^n\bar{\alpha}^n\bar{u}_i^n\epsilon_{,i} - [(\mu_t\bar{\alpha}^n/\sigma_\epsilon) \epsilon_{,i}]_{,i} = \bar{\alpha}^n (\tfrac{\epsilon}{k}) C_1 (G + \Delta G) - \bar{\rho}^n\bar{\alpha}^n (\tfrac{\epsilon}{k})(C_2\epsilon + C_3\Delta\epsilon) \quad (14)$$

where, G, ΔG and $\Delta\epsilon$ are the single phase generation term, extra generation and dissipation terms due to volume fraction and velocity fluctuations [17]. ν_t of the carrier phase is defined as

$$\nu_t = C_\mu k^2/\epsilon \quad (15)$$

where C_μ, C_1, C_2, C_3, σ_ϵ and σ_k are constants of the model [17].

2.2 Inter-Fluid Mass Exchange Model

The different fluids flowing through the submerged plume exchange mass, momentum and energy. The exchange of mass is mainly controlled by evaporation/condensation inside the plume.

Droplets are formed at the interface between the injected gaseous oxidant (SF_6) and the liquid metal bath (Li). The size of the formed droplets is dependent on the critical wavelength of the disturbed gas-liquid interface [18].

This wavelength is a function of the nozzle jet velocity and the liquid phase viscosity and surface tension [18]. The entrained droplets then decrease in size as a result of evaporation. Hence, they flow (in droplet-size space) from a fluid of a larger droplet size to one with smaller droplet size (i.e., from fluid (k+1) to fluid k).

The conservation equations (1 and 4) for fluid k are affected by the evaporation rate $\dot{m}_v^{"k}$, outflow of mass $\dot{m}^{"k}$ and the inflow of mass $\dot{m}^{"k+1}$ due to the decrease in droplet diameter (dD^k/dt). The expressions for $\dot{m}_v^{"k}$ and $\dot{m}^{"k}$, for k $\leq$ n-2, are [19]

$$\dot{m}_v^{"k} = 3\, K_e \bar{\rho}^k / [2(D^k)^2] \tag{16}$$

$$\dot{m}^{"k} = (D^k - \delta D^k/2)^2\, K_e \bar{\rho}^k / [2(D^k)^3 \delta D^k] \tag{17}$$

where, δD^k is the size increment for fluid k and K_e is the forced convection evaporation constant. It can be calculated as [14]

$$K_e = \left[\frac{1 + 0.269\ (Re^k)^{0.581} Pr^{0.33}}{(1 + B)^{0.67}}\right] \frac{8\Gamma}{\bar{\rho}^k}\, \ell n\ (1 + B) \tag{18}$$

where, Pr is the gas film Prandtl number; Γ ($\equiv \mu_\ell/Pr$) is an exchange coefficient; the droplet transfer number B is Cp $(T - T_b^k)/L^k$; Cp is the gas film constant-pressure specific heat; T_b^k and T are the boiling temperatures of fluid k and the gas (fluid n) temperature; L^k is the latent heat of vaporization. Equation (17) can also be used for $\dot{m}^{"k+1}$, the inflow of droplets from k + 1 to k fluid, if k is replaced by k + 1.

As the temperature of combustion products decreases at the end of the plume, new droplets can be formed as a result of condensation. Therefore, mass is transferred from fluid n to fluid n - 1. It is not expected that the

condensed product will evaporate again hence $\dot{m}_v^{'''n-1} = \dot{m}^{'''n-1} = 0$. When k = n, $\dot{m}_v^{'''n}$ = 0 (gas phase) while $\dot{m}^{'''n}$ is interpreted as the condensation rate per unit volume of the gas phase. The latter can be calculated as explained in section 2.5.

Phase Non-Equilibrium Variable

Due to the finite evaporation/condensation rate, the mean mass fraction of the liquid fuel (Li), $\overline{Y}^k$ ($\equiv \overline{\rho}^k\overline{\alpha}^k/\sum_k \overline{\rho}^k\overline{\alpha}^k$), will not be in equilibrium with the corresponding gas phase. Therefore, a mean non-equilibrium variable e may be defined as

$$\overline{e} = [(\overline{Y}_u - \sum_{k=1}^{n-2} \overline{Y}^k)/(\overline{Y}_u - \overline{Y}_e)]_{LL} \tag{19}$$

where $(\overline{Y}_u)_{LL}$ and $(\overline{Y}_e)_{LL}$ are the nonreacting and reacting (equilibrium) liquid Li mass fractions. $(\overline{Y}_e)_{LL}$ is to be obtained from a full equilibrium Li-SF_6 state relationship (e = 1) while $(\overline{Y}_u)_{LL}$ is simply (1 - f), f being the mean mixture fraction.

2.3 The Combustion Model

In the present combustion model, chemistry is assumed fast enough so that the multiphase reacting mixture is in chemical equilibrium. However, the evaporation/condensation rate is not so fast for phase equilibrium to prevail at all points inside the plume. Therefore, the instantaneous state of the reacting mixture is a function of f and the non-equilibrium variable e (Eq. 19).

The time-averaged value of any thermophysical property (ϕ) solely dependent on f and e may be computed as [19]

$$\overline{\phi} = \int_0^1 \int_0^1 \phi(f,e)\ P(f)\ P(e)\ df\ de \tag{20}$$

where P(e) is determined from e as

$$P(e) = (1 - \bar{e})\ \delta(e) + \bar{e}\ \delta(1 - e) \tag{21}$$

and P(f) is the probability density function characterized by $\bar{f}$ and g ($\equiv \overline{f'f'}$). The above two equations yield

$$\bar{\phi} = \int_0^1 [(1 - \bar{e})\ \phi(f,o) + \bar{e}\ \phi(f,1)]\ P(f)\ df \tag{22}$$

where $\phi(f,o)$ is the value of ϕ with no evaporation (e = o) while $\phi(f,1)$ is related to f through full thermodynamic equilibrium state relationships (e = 1).

A beta-function pdf is adopted, namely

$$P(f) = f^{\alpha-1}\ (1 - f)^{\beta-1} / \int_0^1 f^{\alpha-1}\ (1 - f)^{\beta-1}\ df \tag{23}$$

where α and β are given as

$$\alpha = \bar{f}\ [\bar{f}\ (1 - \bar{f})/g - 1] \tag{24}$$

$$\beta = \alpha\ (1 - \bar{f})/\bar{f} \tag{25}$$

$\bar{f}$ and g are to be computed from their transport equations.

2.4 The Multi-Fluid $\bar{f}$ and g Transport Equations

An exact instantaneous two-fluid mixture fraction transport equation was introduced by Chan and Abou-Ellail [16]. This equation can be extended to the multi-fluid case. The modeled MF form reads

$$[\bar{\rho}\ \bar{u}_i \bar{f} - (\Gamma_{f,eff})\ \bar{f}_{,i}]_{,i} = \bar{S}_f \tag{26}$$

where $\Gamma_{f,eff} = \sum_{k=1}^{n} \bar{\alpha}^k\ \mu_\ell^k / S_c + (\bar{\alpha}^n + \sum_{k=1}^{n-1} \bar{\alpha}^k / \sigma^k) \mu_t / \sigma_f$

where $\bar{\rho}$ ($\equiv \sum_k \bar{\rho}^k\bar{\alpha}^k$) is the mixture density; $\bar{u}_i$ ($\equiv \sum_k \bar{\rho}^k\bar{\alpha}^k\bar{u}_i^k/\bar{\rho}$) is the mixture velocity; $\Gamma_{f,eff}$ is an effective exchange coefficient; $\bar{S}_f$ is an additional source/sink term [19] resulting from the interaction of the multi-fluids.

Similarly, the g transport equation can be written as

$$[\bar{\rho}\,\bar{u}_i g - (\Gamma_{g,eff})\, g_{,i}]_{,i} = C_{g1}\,\mu_t\,(\bar{f}_{,i})^2 + \Delta G_g - C_{g2}\bar{\rho}g\epsilon/k \qquad (27)$$

where $\Gamma_{g,eff} = \sum_{k=1}^{n} \bar{\alpha}^k\,\mu_\ell^k/S_c + (\bar{\alpha}^n + \sum_{k=1}^{n-1} \bar{\alpha}^k/\sigma^k)\mu_t/\sigma_g$.

In the above equations, σ_f, σ_g, C_{g1} and C_{g2} are constants of the physical model while ΔG_g is an extra generation/dissipation term [16,19].

The model constants used in the present paper are: $C_\mu = 0.09$, $C_1 = 1.44$, $C_2 = 1.84$, $C_3 = 1.2$, $C_{g1} = 2.8$, $C_{g2} = 1.84$, $\sigma_f = \sigma_g = 0.7$, $\sigma_\alpha^k = 1.0$, $S_c = 0.7$, $\sigma_\epsilon = 1.3$ and $\sigma_k = 1.0$.

2.5 State Relationships

The present MF reacting model utilizes an instantaneous state relationship which is a function of the mixture fraction f and the phase non-equilibrium variable e. A full equilibrium (e = 1.0) state relationship for $Li(\ell)$-$SF_6(g)$ can be constructed. A complete description of the equilibrium computational algorithm, which is mainly based on the Gibbs free-energy minimization approach, is given by Chan et al. [8,9,20].

For the no evaporation case (e = o), the liquid and gas mass fractions and the mixture enthalpy are linearly related to f (i.e. $\phi(f,0) = \phi(0,0)(1-f) + \phi(1,0)f$), as in this case the instantaneous state simply represents a mixing process with no chemical reaction. From the mixture enthalpy, mass fractions of the liquid and gas phases, the mixture temperature and the gas and liquid volume

fractions are then calculated at each value of f for the e = 0 plane. Constant e planes ($o < e < 1.0$) can thus be constructed from the e = 1 and e = 0 planes (e.g., $\phi(f,e) = (1-e)\ \phi(f,0) + e\ \phi(f,1)$).

Figure 1 depicts the overall equilibrium Li(ℓ)-SF_6(g) state relationships, $\phi(f,1)$, at atmospheric pressure and a liquid lithium temperature of 1273 K while the injected SF_6 gas temperature is 298 K. It should be mentioned here that the mixture density and void fraction (gas-phase volume fraction) values given in Fig. 1 are only used in the LHF model calculations. A detailed account of all species concentrations is given by Chan et al. [9]. Since the mean non-equilibrium state is fixed by $\bar{f}$ and $\bar{e}$, $\bar{\alpha}^{n-1}$ of the condensed products can be calculated as follows. First Eqs. (19) and (22) can be used to find $\bar{\alpha}^n$ of the carrier phase

$$\bar{\alpha}^n = \int_0^1 [(1-\bar{e})\ \alpha^n\ (f,0) + \bar{e}\ \alpha^n\ (f,1)]\ P(f)df \qquad (28)$$

where $\alpha^n(f,0)$ and $\alpha^n(f,1)$ correspond to the e=0 and e=1 planes of the states relationships. Since all volume fractions of the liquid Li droplets, $\bar{\alpha}^k$(k=1 to n-2), are to be calculated from Eq. (1), then Eq. (9) can be used to calculate

$$\bar{\alpha}^{(n-1)} = 1 - \sum_{k=1}^{n-2} \bar{\alpha}^k - \bar{\alpha}^n$$

With the value of $\bar{\alpha}^{(n-1)}$, the condensation rate source term $\dot{S}'''^{(n-1)}$ and hence $\dot{m}'''^n (=\dot{S}'''^{(n-1)}/\bar{\alpha}^n)$ can be computed from Eq. (1) for k = n-1.

3. BOUNDARY CONDITIONS

The present predictions are limited to the case of a vertical gaseous SF_6 submerged jet (at 298 K) injected into molten Li (at 1273 K). The nozzle diameter (d) is 2 mm while the inlet gas velocity (u_o) is 325 m/s. The initial

turbulence intensity is taken as 5% of the mean gas velocity while the turbulent length scale is taken as 3% of the injector radius. The surrounding molten Li is assumed stagnant. The entrained mean droplet diameter is estimated [18] as 60 μm. The above data is essentially equivalent to the experimental Li(ℓ)-SF_6(g) combustor data of Parnell et al. [21]. The number of fluids (n) is taken as 6; the first four fluids are dispersed pure liquid Li with mean droplet diameters of 10, 30, 50, 60 μm. Fluid 5 is occupied by the condensing combustion products (70 μm mean droplet diameter) while fluid 6 is only for the gaseous phase. At the nozzle exit plane $\bar{\alpha}^k$ ($k < 6$) = 0 while $\bar{\alpha}^k$ ($k = 6$) = 1.0. At the free stream boundary (gas-liquid interface) $\alpha^1 = \alpha^2 = \alpha^3 = \alpha^5 = \alpha^6 = 0.0$ while $\alpha^4 = 1.0$, since fluid 4 is the only fluid available for the 60 μm entrained Li droplets.

In addition to the multi-fluid (MF) results, similar computations were performed for the LHF model to be used as a basis for comparison. In this case, at the nozzle exit plane, all volume fractions were set equal to zero except for the carrier phase where the volume fraction was set equal to 1.0; the density is taken as that of the mixture.

4. SOLUTION PROCEDURE

The solution procedure is based mainly on an extension of a "multi-fluid SIMPLE" algorithm utilizing an iterative-marching integration technique [13,16,22]. The main variables are $\bar{u}^k_i$, p', k, ϵ, $\bar{f}$, g and $\bar{\alpha}^k$, where p' is a "multi-fluid pressure correction." The submerged jet is overlaid with a non-uniform 2D axisymmetric grid (700 axial x 35 radial nodes). The distances between the radial nodes are varied in proportion to the submerged jet spreading rate.

5. RESULTS AND DISCUSSION

The predicted axial mean profiles of the centerline mixture fraction and normalized axial velocity for the MF and LHF models are depicted in Fig. 2. In Fig. 2, $\bar{u}$, $\bar{u}_g$, $\bar{u}^k$ and $\bar{u}_o$ are axial velocities of the mixture, gas phase, fluid 4 and SF_6 at nozzle exit. The MF model results show that both $\bar{f}$ and $\bar{u}_g$ started to decrease much further downstream ($x/d \simeq 7$) than the corresponding $\bar{f}$ and $\bar{u}_g$ for the LHF model ($x/d \simeq 1.5$). This means that the MF model predicts a much longer plume which is consistent with the experimental data of Parnell et al. [21]. It is interesting to notice that the fluid with 60 μm mean droplet diameter (pure liquid Li) has a peak axial velocity, near $x/d = 6$, which is less than the prevailing gas velocity. However, for $x/d > 70$, $\bar{u}^k$ is larger than $\bar{u}_g$.

The existence of $\bar{u}^k$ in the whole range of x/d shown in Fig. 2 implies that pure liquid Li can penetrate to the centerline of the plume due to finite evaporation rate. Thus, droplets can exist at the centerline even though their volume fraction $\bar{\alpha}^k$ can be very small in the hot region of the plume.

Figure 3 shows the axial profiles of the centerline mean gas temperature T and the mean volume (void) fraction of the gas phase for the MF and LHF models. While the MF model predicted a peak temperature at $x/d \simeq 24$, the LHF model peak temperature occurs at $x/d \simeq 1.5$. The total plume length, which includes reaction, evaporation and condensation zones, is taken at $\bar{\alpha}_g = 0.1$. The present MF model predicts a plume length (L) of approximately 55 nozzle diameters while (L/d) is substantially underpredicted, by the LHF model, to a value of 6. The Parnell et al. data [21] indicated that (L/d) for the $Li(\ell)$-$SF_6(g)$ system is approximately 50 ± 10 depending on the bath temperature, % utilization and the submerged jet orientation with respect to the horizontal direction. Since the MF model predicts a longer plume compared to that of the LHF model, the gradient of $(f_{,1})$ is expected to be smaller and therefore, g calculated from Eq. (27) will

also be smaller resulting in a narrower pdf profile. This explains the higher maximum temperature predicted by the MF model as can be seen in Fig. 3.

Finally, the predicted radial profiles, using the MF model, of the mean temperature and mean mixture fraction are depicted in Fig. 4. for x/d=20. It can be seen from Fig. 4 that the maximum temperature (~3725K) has not reached the center of the plume yet where the temperature is still at 2100 K, i.e., the reaction zone is still longer. At x/d=20 the plume outer radius occurs at r/x~0.18, based on $\bar{f}/\bar{f}_c$ radial profile shown in Fig. 4.

6. CONCLUDING REMARKS

The present multi-fluid (MF) reacting model was used to predict the thermophysical and hydrodynamics of an SF_6 jet submerged in molten Li fuel. The predictions for the plume length is in better agreement with the corresponding experimental data, which could be considered as a substantial improvement over the locally-homogeneous flow (LHF) model. The latter is the only model currently available for the investigation of multiphase submerged combustion.

REFERENCES

1. HUGHES, T.G., SMITH, R.G. AND KILEY, D.H., "Stored Chemical Energy Propulsion System for Underwater Applications," J. of Energy, 7, pp. 128-133, 1983.

2. COOK, L.P. AND PLANTE, E.R., "Survey of Alternate Stored Chemical Energy Reactions," U.S. Department of Commerce Report NBSIR 85-3282, 1985.

3. PARNELL, L.A., EDMUNDS, D.G. AND ROGERSON, D.J., "RTR Studies of Closed Combustion of Liquid Metal Fuels," AIAA-87-1808, AIAA/SAE/ASME/ASEE 23rd Joint Propulsion Conf., San Diego, CA, 1987.

4. PARNELL, L.A., KATZ, D.L., GILCHRIST, J.T., BRYANT, L.E., LUCERO, J.P. AND ZERWEKH, W.D., "Radiography of Liquid Metal Fuel Combustion," Proc. 22nd Intersociety Energy Conversion Eng. Conf., Philadelphia, PA, 1987.

5. LIN, T.F., MAHAFFY, J.H., MANKIN, J.C. AND MILLER, T.F., "Thermal Performances of Oxidant Injections in Submerged Liquid Metal Combustion," 27th JANAF Combustion Subcommittee Meeting, 3, 567-576, 1990.

6. LIN, T.F., "Modelings of Submerged Liquid Metal Combustion," 27th JANAF Combustion Subcommittee Meeting, 3, 577-586, 1990.

7. BLAKE, T.R. AND PARNELL, L.A., "Reacting Gas Jets in Closed Liquid Metal Combustion," 27th JANAF Combustion Subcommittee Meeting, 3, 597-606, 1990.

8. CHAN, S.H., JANKE, P.J. AND SHEN T.R., "Equilibrium Computations of Multiphase Nonideal Electrolytic Systems and Structure of Turbulent Reacting Dissolving Jets," 22nd Symposium (International) on Combustion, The Combustion Institute, pp. 721-729, 1988.

9. CHAN, S.H., TAN, C.C., ZHAO, Y.G. AND JANKE, P.J., "Li-SF_6 Combustion in Stored Chemical Energy Propulsion System," 23rd Symposium (International) on Combustion, The Combustion Institute, pp. 1139-1146, 1990.

10. CHAN, S.H., ZHAO, Y.G., JANKE, P.J. AND TAN, C.C., "Combustion of Turbulent Gaseous Fluorine Jets Submerged in Molten Lithium Fuel," AIAA/ASME Thermodynamics and Heat Transfer Conference, Seattle, WA, 1990.

11. CHAN, S.H. AND SHEN, T.R., "Structure of Turbulent Reacting Gas Jets in Liquids at Elevated Temperatures and Pressures," Int. J. Heat and Mass Transfer, Vol. 33, No. 11, pp. 2503-2509, 1990.

12. ISHII, M., Thermo-Fluid Dynamic Theory of Two-Phase Flow, Eyrolls, Paris, 1975.

13. ABOU-ELLAIL, M.M.M. AND ABOU-ARAB, T.W., "Prediction of Two-Phase Flow and Heat Transfer in Vertical Pipes," Proc. 5th Symposium on Turbulent Shear Flows, Ithaca, NY, pp. 8.1-8.7, 1985.

14. SIRIGNANO, W.A., "Heat and Mass Transfer in Liquid-Gas Spray Systems," Presented at the 1990 ASME Winter Annual Meeting, Dallas, TX, 1990.

15. SIMONIN, O. AND VIOLLET, P. L., "Numerical Modeling of Devolatization of Pulverized Coal Injection Inside a Hot Coflowing Air Flow," Lecture Notes in Engineering (Turbulent Reacting Flows), Springer-Verlag, NY, Vol. 40, pp. 824-846, 1989.

16. CHAN, S.H. AND ABOU-ELLAIL, M.M.M., "A Reacting Two-Fluid Model for Turbulent Two-Phase Diffusion Flames," ASME/JSME Thermal Engineering Proceedings, Vol. 5, ASME 1991, Reno, NV, pp. 95-103, March 1991.

17. MOSTAFA, A.A. AND ELGHOBASHI, S.E., "Effect of Liquid Droplets on Turbulence in a Round Gaseous Jet," NASA Contractor Report - 175063, 1986.

18. CHAWLA, T.C., "Droplet Size Resulting From Breakup of Liquid at Gas-Liquid Interface of Liquid-Submerged Subsonic and Sonic Gas Jets," Int. J. Multiphase Flow, Vol. 2, pp. 471-475, 1976.

19. ABOU-ELLAIL, M.M.M. AND CHAN, S.H., "Modeling of Turbulent Reacting Multi-Phase Flows," 4th Int. Symp. on Transport Phenomena in Heat and Mass Transfer, Sydney, Vol. 1, pp. 391-401, 1991.

20. CHAN, S.H. AND TAN, C.C., "Complex Equilibrium Calculation by Simplex and Duality Theories with Applications to Liquid Metal Fuel Propulsion Systems," Combustion and Flame, Vol. 88, pp. 123-136, 1992.

21. PARNELL, L.A., GILCHRIST, J.T. AND ROGERSON, D.J., "Flash and Real-Time Radiographic Study of Closed Liquid Metal Combustion," 2nd ONR Propulsion Meeting, Irvine, CA, pp. 188-205, October 17-18, 1989.

22. WARDA, H.A. AND ABOU-ELLAIL, M.M.M., "Computer Simulation of Two-Phase Flow in Oil Wells Using Gas-Lift," Engineering Software for Microcomputers, Proc. 1st Int. Conf., Venice, pp. 567-581, 1984.

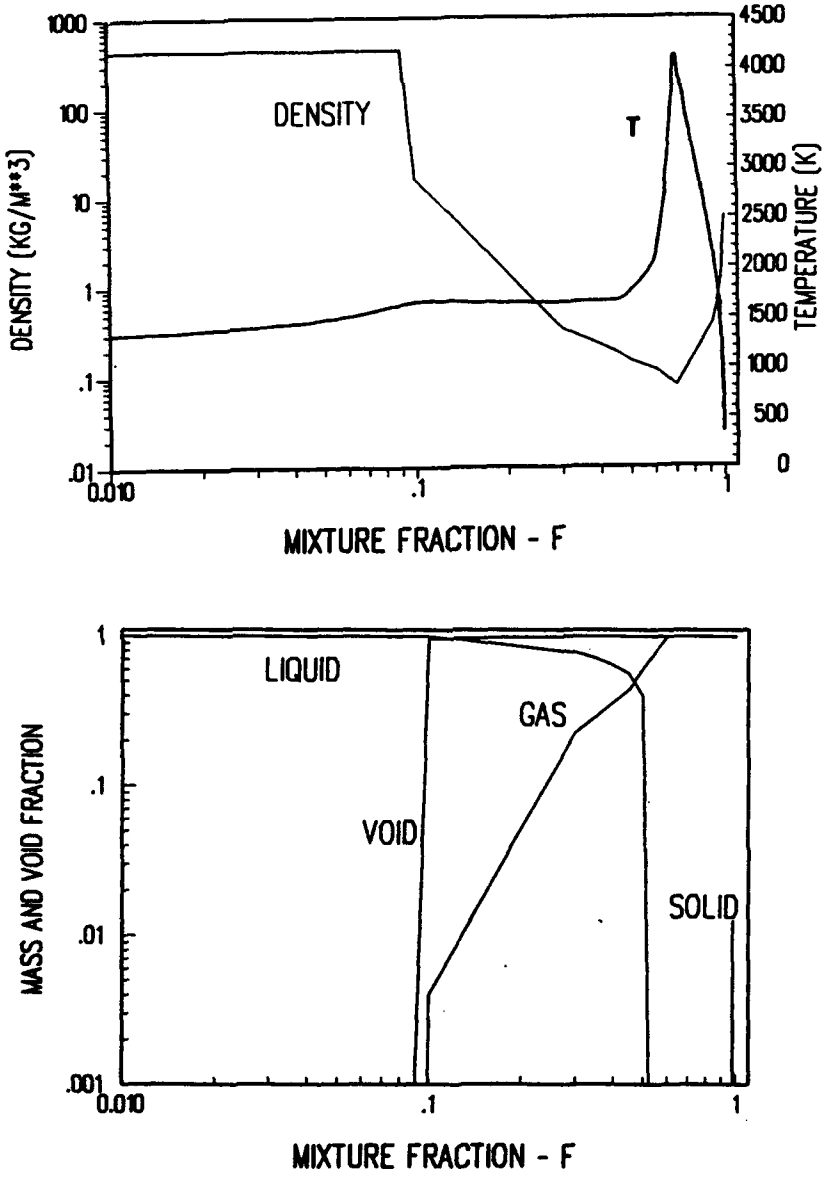

Fig.1 Equations of state for Li - SF_6 system with Li liquid at 1273K and SF_6 gas at 298K.

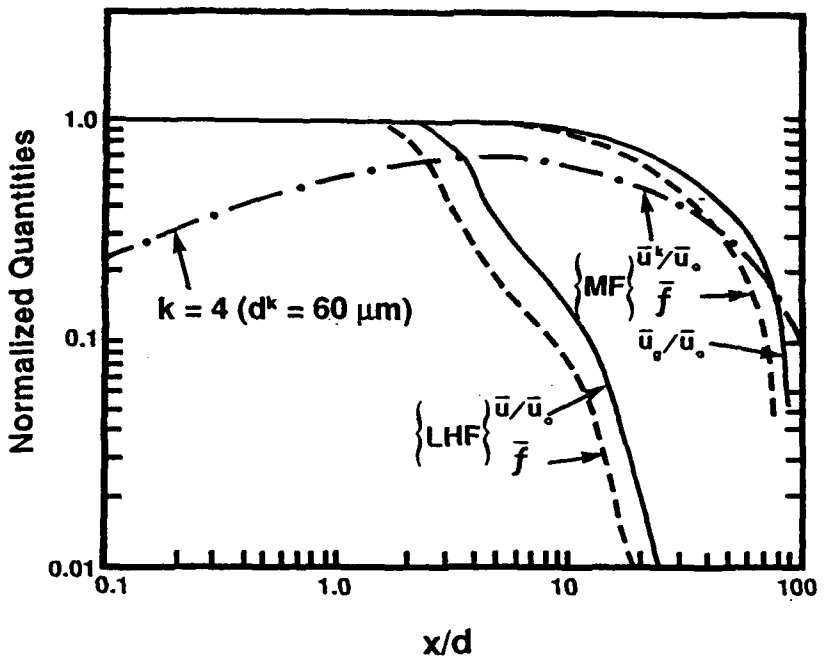

Fig. 2. Axial variation of mean centerline mixture fraction and axial velocity for the MF and LHF models.

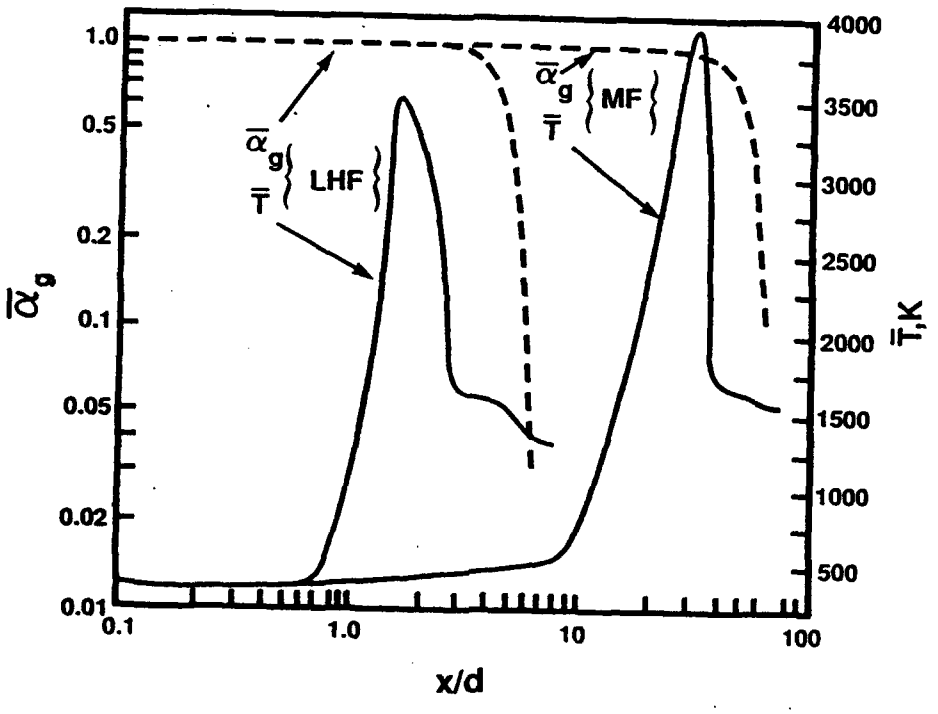

Fig. 3. Axial profiles of the centerline gas temperature and gas volume fraction for the MF and LHF models.

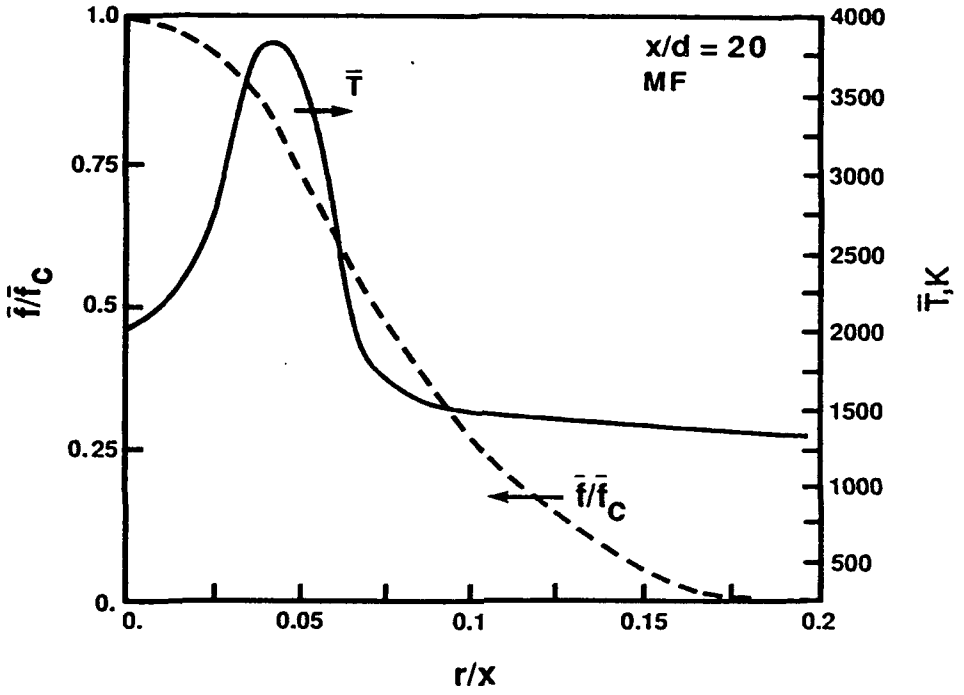

Fig. 4. Predicted radial profiles of the mean mixture fraction and mean temperature for the reacting Li(ℓ)-SF_6(g) system at x/d=20 using the MF model.

ONR REPORT DISTRIBUTION LIST CLOSED,

LIQUID METAL COMBUSTION*

Dr. Gabriel D. Roy (2)
Mechanics Division, Code 1132P
Office of Naval Research
800 North Quincy Street
Arlington, VA 22217-5000

Dr. Richard S. Miller (2)
Mechanics Division, Code 1132P
Office of Naval Research
800 North Quincy Street
Arlington, VA 22217-5000

Dr. Lynn A. Parnell
Naval Ocean System Center
Code 6341
San Diego, CA 92152-5000

Defense Documentation Center (12)
Building 5, Cameron Station
Alexandria, VA 22314

Technical Information Division (6)
Naval Research Laboratory
4555 Overlook Avenue SW
Washington, DC 20375

Dr. Robert Nowark
Chemistry Division
Office of Naval Research
800 North Quincy Street
Arlington, VA 22217-5000

Dr. Albert D. Wood
Technology Programs
Office of Naval Research
800 North Quincy Street
Arlington, VA 22217-5000

Dr. H. W. Carhart
Combustion and Fuels
Naval Research Laboratory
Washington, DC 20375

Professor Allen Fuhs
Department of Aeronautics
Naval Post Graduate School
Monterey, CA 93943

Division Director
Engineering and Weapons
US Naval Academy
Annapolis, MD 21402

Mr. Francis J. Ramano
Code 63R3
Naval Sea Systems Command
Washington, DC 20363

Mr. Robert Tompkins
Code 8122, Bldg. 990/5
Naval Underwater System Center
Newport, RI 02841

Mr. Maurice F. Murphy
Code R33, Room 4-1711
Naval Surface Weapons, White Oak
Silver Spring, MD 20910

Dr. Kurt Mueller
Code R10
Energetic Materials Division
Naval Surface Weapons Center,
White Oak
Silver Spring, MD 20910

---

*One copy except as noted in parentheses.

A1:83_6123e.lst

Dr. Earl Quandt, Jr.
Code 2704
David Taylor Naval Ship
Research and Development Center
Annapolis, MD 21402

Mr. Richard Bloomquist
Code 2752
David Taylor Naval Ship
Research and Development Center
Annapolis, MD 21402

Dr. Lawrence P. Cook
High Temperature Processes Group
National Bureau of Standards
Washington, DC 20234

Professor A. Murty Kanury
Department of Mechanical Engineering
Oregon State University
Corvallis, OR 97331

Professor Irvin Glassman
Department of Mechanical and
Aerospace Engineering
Engineering Quadrangle
Princeton University
Princeton, NY 08544

Dr. W. Lee
Research and Technology Department
Naval Surface Weapons Center
Silver Springs, MD 20703

Professor Norman Chigier
Department of Mechanical Engineering
Carnegie-Mellon University
Pittsburgh, PA 15213

Professor George Janz
Cogswell Laboratory, R306
Department of Chemistry
Rensselaer Polytechnic Institute
Troy, NY 12181

Dr. Leonard Leibowitz
Chemical Technology Division
Argonne National Laboratory
9700 South Cass Avenue
Argonne, IL 60439

Professor Darryl E. Metzger
Department of Mechanical and
Aerospace Engineering
Arizona State University
Tempe, AZ 85281

Professor John Tarbell
104 Fenske Laboratory
Pennsylvania State University
University Park, PA 16801

Professor Thomas E. Daubert
104 Fenske Laboratory
Pennsylvania State University
University Park, PA 16801

Dr. J. Braunstein
Research Division
Oak Ridge Operations
Department E
Oak Ridge, TN 37831

Mr. William J. Greenlee
Engineering Manager Research
Department 741A6, Sundstrand ATG
4747 Harrison Avenue
P.O. Box 7002
Rockford, IL 61125-7002

Professor Gerard M. Faeth
Department of Aerospace Engineering
University of Michigan
Ann Arbor, MI 48109-2140

Mr. Ron Kessing
MS 1207-4P
Fluid System Division
Allied Signal Corporation
1300 West Warner Road
P.O. Box 22200
Tempe, AZ 85285

Dr. Daniel H. Kiely
Power and Energy Group
Pennsylvania State University
Applied Research Laboratory
P.O. Box 30
State College, PA 16801

Mr. Paul M. Dunn/Mr. Christopher J. Egan
Code 804 TH, Bldg. 106
Naval Underwater Systems Center
Newport, RI 02841

Professor John Cimbala
157 Hammond Building
Department of Mechanical Engineering
Pennsylvania State University
University Park, PA 16802

Professor Paul E. Dimontakis
Mail Code 301-46
Graduate Aeronautical Laboratory
California Institute of Technology
Pasadena, CA 91125

Dr. Charles H. Berman
Aerochem Research Laboratories, Inc.
P.O. Box 12
Princeton, NJ 08542

Dr. Donald M. McEligot
Westinghouse Naval System Division
62 Johnny Cake Hill
Middletown, RI 02840

Dr. C. William Kauffman
Department of Aerospace Engineering
The University of Michigan
Ann Arbor, MI 48109-2140

Professor Lea D. Chem
Department of Mechanical Engineering
The University of Iowa
Iowa City, IA 52242

LCDR Mike Barry
NISC - 4311
Naval Intelligence Support Center
4301 Suitland Road
Washington, DC 20390

Mr. David White
Manager of Advanced Development
Solar Turbine, Inc.
2200 Pacific Highway
P.O. Box 85376
San Diego, CA 92138-5376